



International Symposium on Air & Water Pollution Abatement Catalysis (AWPAC) – Catalytic pollution control for stationary and mobile sources

Transition metal loaded TiO₂ for phenol photo-degradation



I. Dobrosz-Gómez^{a,1}, M.Á. Gómez-García^{b,*,1}, S.M. López Zamora^{b,1},
E. GilPavas^{c,2}, J. Bojarska^{d,e}, M. Kozanecki^{d,f}, J.M. Rynkowski^{d,e}

^a Departamento de Física y Química, Facultad de Ciencias Exactas y Naturales, Universidad Nacional de Colombia, Sede Manizales, Campus La Nubia, km 9 vía al Aeropuerto la Nubia, Manizales, Colombia

^b Departamento de Ingeniería Química, Facultad de Ingeniería y Arquitectura, Universidad Nacional de Colombia, Sede Manizales, Campus La Nubia, km 9 vía al Aeropuerto la Nubia, Manizales, Colombia

^c Departamento de Ingeniería de Procesos, Universidad EAFIT, Carrera 49 #7 sur 50, Medellín, Colombia

^d Lodz University of Technology, Zeromskiego 116, 90-924 Lodz, Poland

^e Institute of General and Ecological Chemistry, Lodz University of Technology, Zeromskiego 116, 90-924 Lodz, Poland

^f Department of Molecular Physics, Zeromskiego 116, 90-924 Lodz, Poland

ARTICLE INFO

Article history:

Received 30 November 2014

Accepted after revision 24 March 2015

Available online 9 September 2015

Keywords:

Photo-degradation

Phenol

UV radiation

Visible light

Mo loaded TiO₂

ABSTRACT

Photocatalytic degradation of phenol under both UV radiation and visible light, using TiO₂ (Degussa P-25) and TiO₂ loaded with some transition metal ions (Co, Cu, Fe and Mo) was examined. From the series of metal loaded catalysts, Mo/TiO₂ was the most efficient one. In the presence of Mo, neither TiO₂ anatase/rutile fraction nor its pore size diameter has been affected. However, Mo made its surface more acidic. The percentage of phenol degradation reached under visible light was significantly lower than that under UV radiation due to the lower degree of light absorption by the catalyst surface. From the series of studied catalysts, 2 wt% Mo/TiO₂ was the most efficient one. The synergetic effect between S_{BET}, mean pore size diameter, catalyst agglomerates size, band gap, ZPC and the type of Mo_xO_y species on TiO₂ surface, depending on Mo loading, created its photocatalytic performance.

© 2015 Académie des sciences. Published by Elsevier Masson SAS. All rights reserved.

1. Introduction

Phenols are one of the important organic pollutants discharged into environment causing unpleasant taste and odour to drinking water. They are considered as primary pollutants, being harmful to organisms at low concentrations [1]. At high concentrations, phenol is a toxic and mutagenic substance that may be absorbed even through the skin. The major sources of phenols anthropogenic

inputs into the aquatic environment are wastewaters coming from: production of resins, herbicides, pharmaceutical products, colorants, paints, coal conversion, petroleum and petrochemical industries, etc. One of the most important applications of phenol is its use as an intermediate in the production of phenolic resins. It is also applied in the production of caprolactam (used to the manufacture of nylon 6 and other synthetic fibers) and bisphenol A (manufacture of epoxy resins) [2]. According to the Colombian standards for water quality (NTC-813-2010), the maximum permissible value for phenol in drinking water is 0.001 ppm and along with European Union (EU) directive states, it is of 0.5 ppb (80/778/EC). Consequently, considerable efforts have been devoted to develop a suitable purification method that can easily destroy these biorecalcitrant organic contaminants. However, the application

* Corresponding author.

E-mail address: magomez@unal.edu.co (M.Á. Gómez-García).

¹ Grupo de Investigación en Procesos Reactivos Intensificados con Separación y Materiales Avanzados-PRISMA.

² GIPAB: Grupo de Investigación en Procesos Ambientales.

of conventional methods (activated carbon adsorption, membrane filtration, chemical coagulation purification systems, ion exchange on synthetic adsorbent resins, etc.) also generates wastes whose treatment requires additional steps and costs.

In recent years, the heterogeneous photocatalytic oxidation processes, employing TiO_2 and UV radiation, have emerged as a promising alternative for the degradation of persistent organic pollutants, producing more biologically degradable and less toxic substances [1,2]. The photocatalytic phenol oxidation is initiated by the absorption of the photon with energy equal to or higher than the band gap of TiO_2 , producing an electron–hole pair on its surface. Next, a photogenerated electron is promoted to the conduction band while a positive hole is formed in the valence band. Excited state electrons and holes can recombine and dissipate the input energy as heat, get trapped in metastable surface states, or react with electron donors and electron acceptors adsorbed on the semiconductor surface or within the surrounding electrical double layer of the charged particles [1]. After the reaction with water, these holes can produce hydroxyl radicals with high redox oxidizing potential. The main reaction site for phenol destruction is bulk liquid, where the attack of hydroxyl radicals on the carbon rings results in the formation of various oxidation intermediates [2]. Hydroquinone, catechol, and *p*-benzoquinone are reported as the most frequently formed intermediates [2]. Moreover, chlorohydroquinone, 4-chlorocatechol and resorcinol can be converted to acetylene, maleic acid, carbon monoxide and carbon dioxide.

TiO_2 (Degussa P-25) is the most widely used photocatalyst since it presents high activity under UV radiation, biological and chemical non-toxicity, stability, availability and low cost. However, its photo-response under visible light is not so efficient, since only 3–5% of the solar spectrum is in the UV range. Moreover, its photocatalytic properties can be limited by stabilization of the charge photocarriers in the bulk of the material, by fast charge recombination either in the bulk or at the surface of the oxide and/or by its relatively large band gap [3]. Several strategies have been used to reduce electron–hole recombination rates and to increase photocatalytic efficiency of TiO_2 under visible light, among them doping/loading with metal [2,4] or non-metal [5,6] ions. Recently, a number of papers have been published focusing on the photo-degradation of phenolic compounds [1,7]. A lot of them were related to the application of TiO_2 as photocatalyst [7,8]. In the light of the reviewed researches, one can see that the comparison among the results reported in the literature is extremely difficult since conditions (such as: initial pH of solution, type and concentration of used oxidation agent, wavelength light irradiation, reactor geometric configuration, catalyst loading, etc.) at which the experiments were carried out, were very different. Moreover, the origin and the crystalline structure of TiO_2 , affecting its electronic and physicochemical properties, also strongly influence its photoactivity [2,8]. When doped TiO_2 was applied as a catalyst, the preparation methods and metal loading used by different researches for the catalysts synthesis were usually different [1,2]. All these

factors can be the origin of the discrepancies found in the literature when dealing with TiO_2 loaded materials. Therefore, the application of the same bare TiO_2 as the starting material, its subsequent modification with metals using the same procedure, and finally their evaluation under the same experimental conditions can be considered as an alternative to assess their real effect on TiO_2 properties and photoactivity.

This paper presents the results of phenol photo-degradation under both UV radiation and visible light, using TiO_2 (Degussa P-25) and TiO_2 loaded with some transition metal ions (cobalt, copper, iron, and molybdenum). The samples were prepared by the wet impregnation method. Their characterization was carried out performing thermal analysis (TG-DTA-MS), N_2 physisorption (BET), scanning electron microscopy (SEM-EDS), atomic absorption spectroscopy (AAS), X-ray diffraction (XRD), Raman spectroscopy (RS), diffuse reflectance spectroscopy (DRS), and measuring their zero point charge (ZPC). The aim of this work was to understand the role of various structural, morphological, physicochemical and optical properties and to evaluate their relative effect on photocatalytic activity in phenol degradation (batch system). Thus, from the group of four transition metals, the most promising (active) one was selected and its loading was optimized.

2. Experimental

2.1. Materials

Commercial TiO_2 (Degussa P-25, purity > 99%), iron (III) nitrate 9-hydrate ($\text{Fe}(\text{NO}_3)_3 \cdot 9\text{H}_2\text{O}$, PanReac, purity $\geq 98\%$), cobalt (II) nitrate 6-hydrate ($\text{Co}(\text{NO}_3)_2 \cdot 6\text{H}_2\text{O}$, PanReac, purity $\geq 98\%$), copper (II) nitrate 3-hydrate ($\text{Cu}(\text{NO}_3)_2 \cdot 3\text{H}_2\text{O}$, PanReac, purity $\geq 98\%$), and ammonium molybdate 4-hydrate [$(\text{NH}_4)_6\text{Mo}_7\text{O}_{24} \cdot 4\text{H}_2\text{O}$, purity $\geq 99\%$] were used as starting materials. First, transition metal loaded TiO_2 (M/ TiO_2), with a metal nominal content of 1 wt%, were prepared by incipient wet impregnation method. Next, the series of catalysts containing 0.5–5 wt% of the most promising metal was synthesized, using the same method. Each time, the desired amount of corresponding metal precursor was dissolved in deionized water and next TiO_2 (Degussa P-25) was added. After stirring at room temperature for 24 h, the solvent was evaporated under reduced pressure (100 mbar) at 75 °C. The as-prepared catalyst precursors were dried in an oven at 100 °C for 12 h and calcined at 500 °C for 6 h, according to TG-DTA-MS analysis (not shown here, in details described in [9]).

2.2. Characterization methods

X-ray diffraction (XRD) patterns were obtained at room temperature using a Rigaku, Miniflex II diffractometer, operating at 30 kV and 15 mA ($\text{Cu K}\alpha$ radiation, $\lambda = 1.540562 \text{ \AA}$). Data were collected in the range of 20–90° 2θ , with a step size of 0.01678 and step time of 10 s. The standard diffraction data from JCPDS files of anatase (No. 21-1272) and rutile (No. 21-1276) were used to identify

phase composition. The particle size (D_{hkl}) was estimated from the width of the principal diffraction peak (101) of anatase phase using the Scherrer equation:

$$D_{hkl} = \frac{k\lambda}{\beta \cos\theta} \quad (1)$$

where θ is the incidence angle for hkl reflection (rad); the hkl values are Miller indices parameters; each index denotes a plane orthogonal to a direction (hkl) on the basis of the reciprocal lattice vectors (but not always normal to this direction in Cartesian coordinates, since the reciprocal lattice vectors are not necessarily perpendicular to each other), β is the angular line width at medium height (rad) and k corresponds to the Scherrer constant (0.9). The lattice parameters ($a = b \neq c$) were obtained for (101) crystal plane of anatase phase, according to the following equation (corresponding to tetragonal crystalline structure):

$$\frac{1}{d^2} = \frac{h^2 + k^2}{a^2} + \frac{l^2}{c^2} \quad (2)$$

considering the interplanar spacing (D_{hkl}), the distance between adjacent planes in the set (hkl), can be determined using the Bragg Law:

$$D_{hkl} = \frac{\lambda}{2\sin\theta} \quad (3)$$

The cell volume (tetragonal one) was determined as follows:

$$V = a^2c \quad (4)$$

where a and c are lattice parameters.

Finally, the anatase and rutile fractions were determined by Eq. (5) where I_A and I_R are the integrated intensities of the most intense peaks of anatase (101) and rutile (110) phases:

$$X_A = \frac{0.79I_A}{0.79I_A + I_R} \quad (5)$$

Scanning electron microscopy (SEM) measurements were performed by S-4700 microscope (Hitachi, Japan) coupled with energy dispersive spectrometer (EDS) (Thermo Noran, USA) at an acceleration voltage of 25 kV. Images were recorded at several magnifications. The content of elements in the studied micro-area of the oxide surface layer was determined by the EDS method, based on the obtained characteristic X-ray spectra. In order to reduce the charge build-up on the samples, they were placed on carbon plasters in a holder and before analyzing were coated with a carbon monolayer.

Raman spectroscopy was performed by a Raman spectrometer (model T-64000, Jobin-Yvon) coupled with microscope (Olympus BX-40), using three grids (3×1800 grove/mm). The system offers spectral resolution of 1 cm^{-1} for exciting line of 514.5 nm and spatial definition lower than $1 \mu\text{m}$ on the sample surface. The measurements were carried out at opened confocal diaphragm, long focal distance with 50 times magnification and numerical aperture $NA = 0.5$. Each time, the signal was collected from area with a diameter of ca. 4–5 μm . The

time of measurement was adjusted to obtain a spectrum characterized by sufficient signal-to-noise ratio for the correct mathematical analysis (deconvolution). Several independent spectra for each sample were collected (between 3 and 7). The deconvolutions of the spectra have been carried out using PeakFit software (version 4.0, Jandel).

Atomic absorption spectroscopy (AAS) analyses were performed with a Solaar M6 Unicam spectrometer in order to estimate the amount of metal loaded on TiO_2 . Initially, the microwave digestions of the analyzed samples were carried out in aqua regia ($3 \text{ cm}^3 + 100 \text{ mg}$ of the sample), using microwave oven MLS-1200 MEGA (Milestone). The obtained solutions were placed in measuring flasks and diluted with 100 cm^3 of deionised water. A blank test was prepared in the similar way.

Nitrogen adsorption-desorption isotherms were measured at -196°C using Micromeritics ASAP 2010 apparatus (Carlo Erba). Prior to the measurements, the samples were degassed for 4 h at either 300°C (M/TiO_2) or 100°C (TiO_2). The specific surface area (S_{BET}) was calculated using BET equation. The pore size, their distribution and the pore volume were estimated using the Barret–Joyner–Halenda (BJH) method.

Zero point charge (ZPC) of studied powders was determined by mass titration (MT) method [10,11]. It involves finding the limiting pH value of catalyst/water slurry, as the catalyst content is constantly increased. Different amounts of powders were added to deionized water in the following weight ratios: 0.1, 1, 5, 10, and 20%. The resulting pH values were measured after 24 h of equilibrium, at room temperature.

UV–VIS diffuse reflectance spectra (DRS) were recorded by a PerkinElmer Lambda 20 UV–VIS spectrophotometer coupled with a diffused reflectance sphere, in the range of 190–800 nm at 240 nm/min, in order to determine the band gap of the studied samples. UV–VIS diffused reflectance spectra (DRS) were transformed to $F(R)$ using the Kubelka–Munk expression, Eq. (6). To establish the type of band-to-band transition in the synthesized powders, the absorption spectra were fitted to equations for indirect band gap transitions. Next, the Tauc plot: $[F(R) \cdot h\nu]^{1/2}$ vs. photon energy, $h\nu$, Eq. (7), was done. Finally, the band gap values were obtained extrapolating the linear part of the plot $[F(R) \cdot h\nu]^{1/2}$ vs. photon energy, Eq. (8), assuming the porous samples as indirect crystalline semiconductors [5,12]:

$$F(R) = \frac{(1 - R)^2}{2R} \quad (6)$$

$$h\nu = \frac{hc}{\lambda} = \frac{1239.84}{\lambda} \quad (7)$$

$$(F(R)h\nu)^{\frac{1}{2}} = A(h\nu - E_g) \quad (8)$$

Phenol photocatalytic degradation tests were carried out in a Pyrex batch cylindrical reactor containing ca. 120 mL of an aqueous phenol solution (20 ppm), with a pH of 5 (natural pH), and TiO_2 (as received, without any further treatment) or M/TiO_2 catalyst (0.5 g/L). Air was continuously bubbled (10 mL/s) to the agitated solution

(350 rpm). In order to distinguish the loss of phenol through adsorption phenomena from the oxidative photo-degradation, each time, the corresponding catalyst suspension was constantly stirred for 30 min in the darkness before irradiation. Next, 1 mL of the sample was taken and the initial concentration of phenol was determined (C_0). Thus, it was assumed that independently of the studied catalyst (its ZPC) and its phenol adsorption capacity, the C_0 value, taken after 30 min in the darkness, was the initial phenol concentration in the solution. Subsequently, a corresponding lamp used as a source of UV radiation or visible light was introduced into the reactor. Therefore, a black light tubular lamp (maximum light intensity at $\lambda = 365$ nm, 15 mm of diameter, 265 mm of length, model F8T5/BL Philips, 8 W, photon flux of 1.47×10^{19} 1/m²/s, radiant flux of 0.58 mW/cm²) or day light tubular lamp (maximum light intensity at $\lambda = 470$ nm, 15 mm of diameter, 265 mm of length, model F8T5/D Philips, 8 W, photon flux of 1.89×10^{19} 1/m²/s, radiant flux of 0.74 mW/cm²) was applied. The reaction was kept running for 2 h at room temperature (25 °C). Each time, 1 mL samples were taken at intervals of 15 or 30 min. The evolution of phenol concentration was followed by high-pressure liquid chromatography (HPLC). A HPLC-UV, AGILENT, was used with the following parameters: mobile phase: acetonitrile–water–acetic acid (36:60:4), flow: 0.8 mL/min, lamp: tungsten–deuterium, column: ECLIPSEXDB-C18-5 mm, and retention time: 10 min. The percentage of phenol degradation (% Deg) was calculated after 120 min of reaction as follows:

$$\% \text{ Deg} = \frac{C_0 - C_f}{C_0} \quad (9)$$

where C_0 and C_f are the initial and final phenol concentrations, respectively. The blank tests were also performed, at the same conditions as reaction, in the absence of catalyst. Negligible phenol degradation was observed in experiments performed both under UV radiation and visible light.

3. Results and discussion

3.1. Physicochemical properties and catalytic performance of M/TiO₂ catalysts

Table 1 reports the results of AAS, S_{BET} , ZPC and Band gap determined for TiO₂ and M/TiO₂ catalysts.

Table 1
Characterization of TiO₂ and M/TiO₂ catalysts.

Catalyst	Real metal content (%) ^a	S_{BET} (m ² /g) ^b	V_p (cm ³ /g) ^b	D_p (nm) ^b	ZPC ^c	Band gap (eV) ^d
TiO ₂	–	57	0.429	37.5	6.6	3.09
Co/TiO ₂	1.02	55.5	0.185	15.2	7.3	3.05
Cu/TiO ₂	0.98	56.2	0.406	20.8	7.1	3.00
Fe/TiO ₂	1.05	56.9	0.420	29.0	6.9	2.85
Mo/TiO ₂	0.99	56.1	0.430	37.6	6.0	2.90

S_{BET} : Specific surface area determined by BET method; V_p : pore volume taken at $p/p_0 = 0.99$; D_p : average pore diameter determined by the BJH method.

^a Determined by AAS.

^b Determined by N₂-BET.

^c Determined by MT.

^d Determined by UV–VIS DRS.

For all M/TiO₂ samples, the real metal content was very close to the nominal one (1 wt%). Fig. 1 shows the representative N₂ adsorption-desorption isotherms of TiO₂ and M/TiO₂ catalysts. All five analyzed samples showed type IV isotherms, according to the IUPAC classification, with hysteresis loops (type A, according to de Boer, or H1) typical of mesoporous materials. The hysteresis loop is associated with the capillary condensation taking place in the mesopores signifying the preservation of the mesoporous structure even after calcination at elevated temperature. The type A hysteresis loop is attributed to the cylindrical shaped pores. A typical pore size distribution for all studied catalysts is included in Fig. 1. All samples exhibit a unimodal pore size distribution.

One can see that the S_{BET} of M/TiO₂ catalysts were very similar to that of TiO₂ (57 m²/g). However, impregnation of TiO₂ with Fe, Cu and Co species reduced its mean pore size diameter (22.7%, 44.5%, and 59.5%, respectively). We assume that some obstruction of TiO₂ pores by metal oxidic species can take place, considering that TiO₂ impregnation with metal ions consists of their interactions with the support, by physical and/or chemical adsorption, decomposition and oxidation during calcination process. On the other hand, the mean pore size diameter of Mo/TiO₂ was very similar to that of TiO₂.

The ZPC represents the value of pH at which the coverage of catalyst surface with H⁺ equals that with OH[−] (zero net surface charge), taking into account both the acidic and basic sites. It allows determining both the propensity of the catalyst surface to be charged either positively or negatively, as a function of the pH, and its capacity to the ion exchange with contaminant present in the solution. The ZPC of TiO₂, determined experimentally in this study, was 6.6. The impregnation of TiO₂ with Fe, Cu, and Co species led to the shift of its ZPC to more basic values (Table 1). It could be related to the presence of different metal oxides (Fe_xO_y, Cu_xO_y, Co_xO_y) on TiO₂ surface, characterized by a lesser acid nature than that of titania. On the other hand, for Mo/TiO₂ system, the ZPC showed a more acidic character than that of the support, indicating surface enrichment with the species characterized with an acidic behavior, such as Mo_xO_y.

The determined band gap of TiO₂ equaled 3.09. This value is very close to that reported in the literature (3.01 eV) for TiO₂–Degussa P-25 [13]. The impregnation of TiO₂ with metal species reduced its band gap, showing a red shift into lower eV (Table 1). The highest red shift was

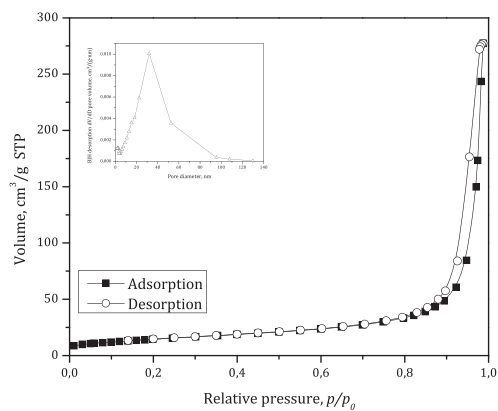
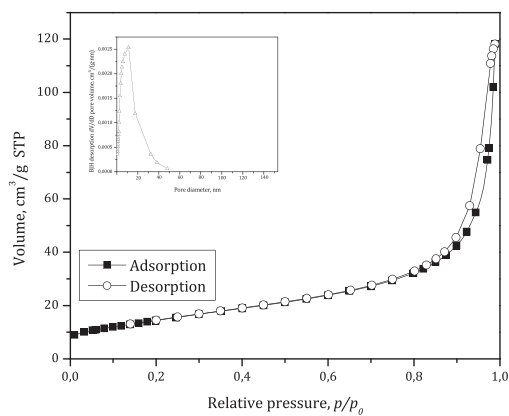
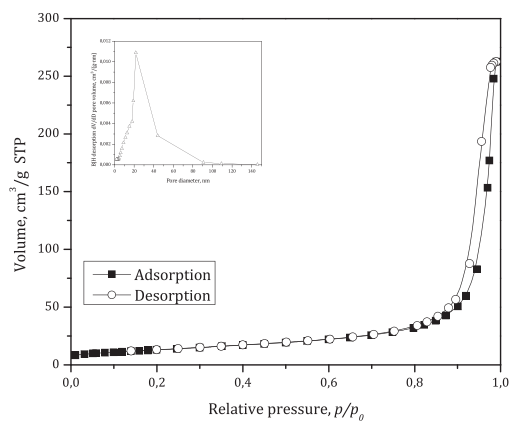
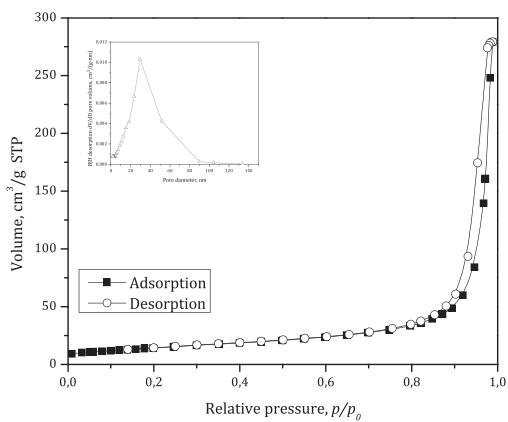
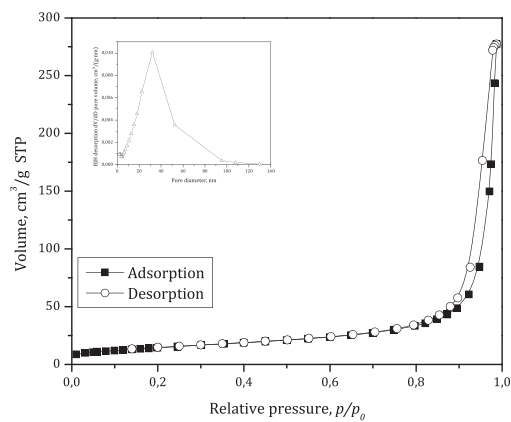
TiO₂1% Co/TiO₂1% Cu/TiO₂1% Fe/TiO₂1% Mo/TiO₂

Fig. 1. The representative N₂ physisorption isotherm and BJH pore size distribution of TiO₂ and M/TiO₂ catalysts.

observed for Fe/TiO₂ catalyst. The effect of metal presence on TiO₂ band gap reduction can be attributed to:

- the charge-transfer transitions between the metal ion d electrons and the TiO₂ conduction or valence band;
- the generation of impurity levels in the band gap of TiO₂; if these states lie close to the band edges, they can overlap band states, narrowing its band gap [14];
- the creation of allowed energy states in the band gap of TiO₂, as a consequence of the presence of segregated M_xO_y clusters on its surface [15], that can induce photoactive transitions in visible light, due to an excitation of an electron from this energy level into the TiO₂ conduction band. Therefore, the presence of metal species can affect TiO₂ photoactivity altering the electron–hole pair recombination rate.

SEM–EDS micrographs of TiO₂ and M/TiO₂ catalysts are presented in Fig. 2 and Appendix 1. They do not reveal any significant differences in the morphology of TiO₂ and M/TiO₂ catalysts. All samples were characterized with the presence of aggregates with irregular shapes and sizes in the range of 3.5–30 μm. The following order of average size of catalysts agglomerates, depending on the supported metal, was observed: Co/TiO₂ (5 μm) < Mo/TiO₂ (8 μm) < Cu/TiO₂ (10 μm) < Fe/TiO₂ (15 μm) < TiO₂ (30 μm). One can see that the presence of metal prevents TiO₂ particles agglomeration probably due to the change in the surface charge of the catalysts. It is important since big aggregates can be detrimental to photocatalytic activity, being hidden for light absorption. For all samples, the presence of uniformly distributed metals was confirmed by EDS measurements.

The XRD pattern of TiO₂ (not shown here) corresponded to the mixture of anatase and rutile crystalline phases, in the ratio of ca. 5.6:1, respectively. The anatase to rutile ratio was determined using areas of the most intense diffraction peaks corresponding to anatase (2θ = 25.3, 37.8 and 48.0) and rutile (2θ = 27.4, 36.1 and 54.3) crystalline phases of titania [11]. The diffraction patterns of M/TiO₂ catalysts were

very similar to that of TiO₂ (not shown here). No clear metal and/or metal oxides reflections were observed. It could be related to:

- the overlapping peaks descended from anatase/rutile phases with these suitable for metal phases;
- relatively low metal content (1 wt%) and its uniform distribution on the TiO₂ surface;
- and/or the amorphous nature of the metals.

Table 2 presents the average crystallite size, lattice parameters (*a*, *b*, *c*, and *d_{hkl}*) and anatase to rutile ratio for TiO₂ and M/TiO₂ catalysts. The lattice parameters for M/TiO₂ systems are very close to those of TiO₂, suggesting good dispersion of metal species on the TiO₂ surface and/or on a few top layers of TiO₂ particles. Moreover, the average crystallite size of all M/TiO₂ catalysts was similar to that of TiO₂. Finally, the following order of anatase to rutile ratio was found: Cu/TiO₂ < Co/TiO₂ < Mo/TiO₂ < TiO₂ < Fe/TiO₂, suggesting that Cu, Co and Mo can act as promoters of anatase to rutile phase transformation, while Fe can be its inhibitor. In order to determine if the observed changes in anatase/rutile ratio and crystallite size are attributed to the presence of metals on TiO₂ surface, the XRD studies of thermally treated TiO₂ (dried and calcined as catalysts) were performed. The slight effect of temperature on both anatase/rutile ratio and crystallite size was observed (Table 2).

In the absence of dopants or impurities, the sufficient thermal energy required to anatase to rutile phase transformation can be reached at ca. 700 °C [16]. Various cationic dopants have been studied in terms of their effect on the kinetics of the anatase to rutile transition. It was concluded that cations characterized by small radii and low valence (< 4) accelerate the transition to rutile due to the increase in oxygen vacancies that result from the assumed substitution of Ti⁴⁺ ions with cations of lower valences. On the other hand, when cations of high valence (> 4) are assumed to substitute the Ti ions in the anatase lattice, this gives rise to the annihilation of existing oxygen

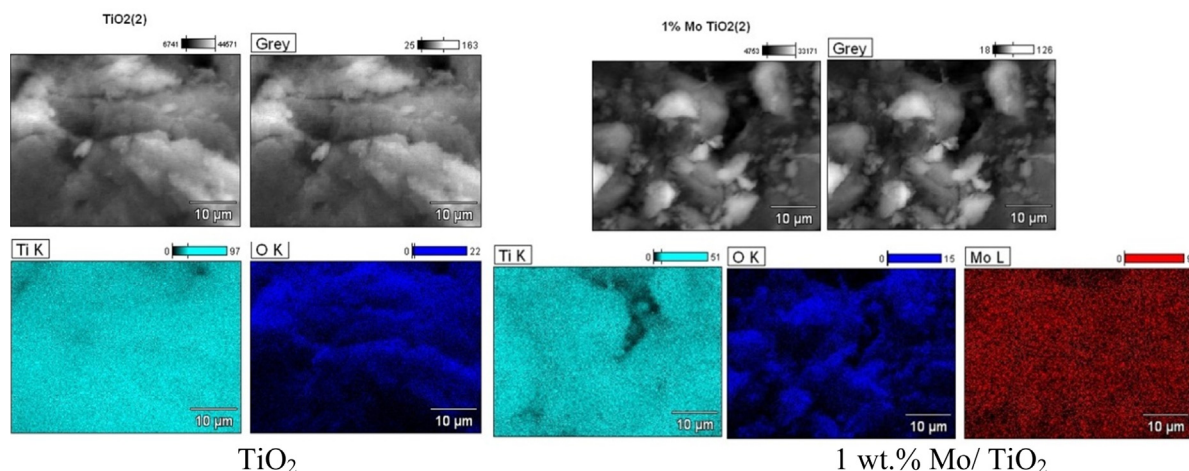


Fig. 2. (Color online.) Back-scattered electron (BSE) photomicrographs and EDS maps of TiO₂ and 1 wt% Mo/TiO₂ catalysts (Magnification: × 2500).

Table 2The average crystallite size, lattice parameters, and anatase to rutile ratio of TiO₂ and M/TiO₂ catalysts.

Catalyst	d_{hkl} (Å)	$a = b$ (Å)	c (Å)	Cell volume (Å ³)	Crystallite size (nm)	Anatase fraction	Anatase/rutile ratio
TiO ₂ (as received)	3.5	3.8	9.8	141.5	20.7	85.0%	5.6
Co/TiO ₂	3.5	3.8	9.2	132.8	20.0	83.3%	5.0
Cu/TiO ₂	3.5	3.8	9.5	137.2	21.0	81.3%	4.3
Fe/TiO ₂	3.5	3.8	9.3	134.3	18.9	85.6%	6.0
Mo/TiO ₂	3.5	3.8	9.4	135.7	20.6	83.7%	5.1
TiO ₂ (calcined)	3.5	3.8	9.8	141.5	20.3	84.0%	5.3

vacancies and the formation of Ti interstitials of the same or lower valence. These processes can be viewed in light of the inertia to alteration (through ionic transport) of the relatively large and rigid oxygen sublattice, which largely determines the structural stability and the capacity to reorganize the chemical bonds to form rutile. According to the literature, Co, Cu [16] and Mo [17] have already been reported as promoters and Fe [16] as an inhibitor of anatase to rutile phase transformation.

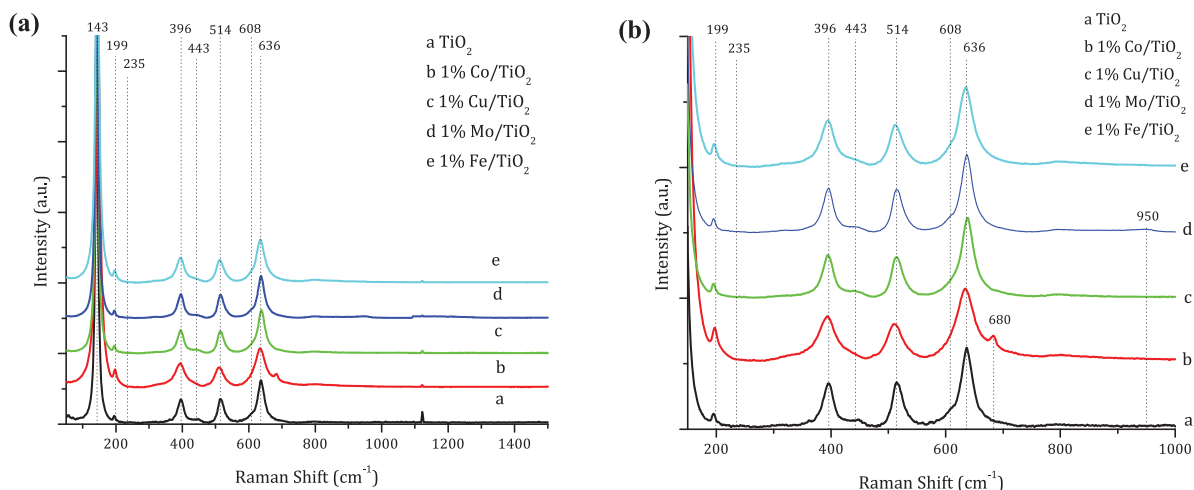
Fig. 3 presents Raman spectra of TiO₂ and M/TiO₂ systems. For TiO₂, the peaks centred at 143, 199, 396, 514 and 636 cm⁻¹ correspond to its anatase crystalline phase, while these located at 235, 443, 608 and 826 cm⁻¹ are characteristic of the rutile one. These peaks can be also observed in the spectra of M/TiO₂ catalysts.

Moreover, for Co/TiO₂ two new shoulders at 680 and 480 cm⁻¹ were registered and can be assigned to the presence of CoO and Co₃O₄ species [18]. The spectrum of Mo/TiO₂ catalyst also exhibited a new peak at 950 cm⁻¹, characteristic of Mo-oxide species supported on TiO₂ [19]. It can be attributed to the mixture of phases based on [Mo₇O₂₄]⁶⁻ and [Mo₅O₁₇]⁴⁻ ions [20]. On the other hand, for Cu/TiO₂ and Fe/TiO₂ catalysts, no characteristic peaks corresponding to their metal oxides were found. In the case of Cu/TiO₂, the band near 293 cm⁻¹, characteristic of the CuO crystalline phase, can be expected [21]. For Fe/TiO₂,

the series of peaks at 225, 247, 293, 299, 412, 498 and 613 cm⁻¹, characteristic of Fe₂O₃, should be present [22]. Thus, their absence is probably due to their overlapping by TiO₂ peaks, characteristic of anatase and rutile crystalline phases.

Fig. 4a summarizes the results of phenol photo-degradation under UV radiation in the presence of TiO₂ or M/TiO₂.

After 2 h of experiment, the following order of activity was observed: TiO₂ (89.6%) > Mo/TiO₂ (78.6%) > Fe/TiO₂ (30.1%) > Cu/TiO₂ (18.6%) > Co/TiO₂ (11.2%). One can see that deposition of transition metal ions on TiO₂ surface was detrimental to its photoactivity in phenol degradation. However, significant differences in their photocatalytic behavior were observed, due to their different physico-chemical, textural, and electronic properties. The impregnation of TiO₂ with Fe, Co, or Mo let to obtain well-crystallized mixtures of anatase and rutile phases with a similar S_{BET} and crystallite size. However, its loading with Cu allowed us to obtain a catalyst with a significantly lower amount of anatase fraction, probably due to the surface dehydroxylation caused by anatase to rutile phase transformation. Consequently, its activity was significantly reduced since dehydroxylation reduces hole trapping by surface hydroxyls, enhancing recombination and oxygen and/or phenol species adsorption. On the other hand, the

**Fig. 3.** Representative Raman spectra for TiO₂ and M/TiO₂, (a) 50–1400 cm⁻¹; (b) 200–1000 cm⁻¹ (enlarged view of Fig. 3a).

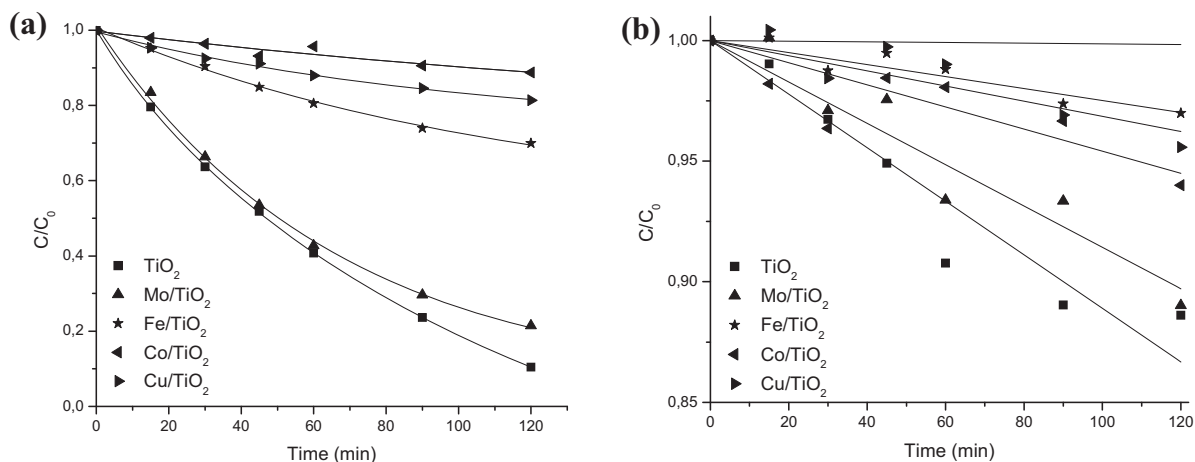


Fig. 4. The photocatalytic degradation of phenol over TiO_2 and M/TiO_2 catalysts under: (a) UV radiation and (b) visible light ($C_{\text{phenol}} = 20$ ppm, $\text{pH} = 5$, $C_{\text{cat}} = 0.5$ g/L).

enrichment of TiO_2 surface with different metal species, not detected by XRD but confirmed by AAS, SEM-EDS, and/or Raman spectroscopy, indicated imperfect diffusion of metal ions into TiO_2 due to the low temperature of catalysts preparation and calcination. Finally, surface acidity was also found as an important factor in determining the efficiency of studied photo-catalysts. The systems containing Fe, Cu or Co species, characterized by their basic nature (CuO , CoO , Co_3O_4 , Fe_2O_3 , etc.) and ZPC higher than that of TiO_2 , were found to be less active in phenol photo-degradation. In contrast, TiO_2 enrichment with acidic species introduced by Mo impregnation and based on $[\text{Mo}_7\text{O}_{24}]^{6-}$ and $[\text{Mo}_5\text{O}_{17}]^{4-}$ ions showed higher activity indicating its beneficial role in the creation of active centers for phenol adsorption.

Fig. 4b summarizes the results of phenol photo-degradation under visible light in the presence of TiO_2 or M/TiO_2 . The following order of activity was determined: TiO_2 (11.4%) \approx Mo/TiO_2 (11%) $>$ Co/TiO_2 (6%) $>$ Cu/TiO_2 (4.4%) $>$ Fe/TiO_2 (3%). One can see that the percentage of phenol degradation reached under visible light is significantly lower than that under UV radiation. Since light intensity determines the extent of light absorption by the semiconductor surface at a given wavelength, the rate of the photocatalytic initiation of electron-hole formation in the photochemical reaction will be strongly dependent on light intensity. Considering that in visible light the number of photons per unit of time that can strike the catalysts surface is higher than that under UV radiation, higher photoactivity can be expected. However, in visible light, the photon energy is noticeably lower. Therefore, the degree of light absorption by the catalyst surface will also be strongly reduced, leading to a lower percentage of degradation. Since the excitation of band gap electrons with 365 nm can promote them to the conduction bands with higher kinetic energy, they can reach the solid-liquid interface more easily, suppressing electron-hole recombination. Moreover, the value of the band gap of undoped TiO_2 (3.09) also confirms that it cannot be excited under

visible light. It was also observed that the catalysts characterized by bigger agglomerates size showed lower activity under visible light. Consequently, the presence of big aggregates was found to be detrimental to phenol photo-degradation, since catalyst particles were hidden for light absorption.

Resuming, one can see that TiO_2 loading with transition metal ions can be detrimental to its photoactivity in phenol degradation. However, from the series of studied catalysts, Mo/TiO_2 was the most efficient one. The presence of different Mo_xO_y phases allowed us to obtain both more efficient charge separations due to new energy level produced in the band gap of TiO_2 and an Mo-donor level below TiO_2 conduction band, leading to the reduction in TiO_2 band gap. Thus, the probability of electron-hole recombination on Mo/TiO_2 surface can be reduced. As the next step, the optimization of Mo loading on TiO_2 surface will be discussed.

3.2. Physicochemical properties and catalytic performance of 0.5–5 wt% Mo/TiO_2 catalysts

Table 3 reports the results of AAS, S_{BET} , ZPC, and band gap determination for TiO_2 and x wt% Mo/TiO_2 catalysts.

For all Mo/TiO_2 systems, the real metal content was very close to the nominal one (0.5–5 wt%).

As molybdenum content increased, S_{BET} and mean pore size diameter of the studied catalysts decreased (Table 3). It can be related to both TiO_2 pores obstruction due to the imperfect diffusion of metal ions into the support, at a temperature at which catalysts were calcined, and powders sintering favoured by the increasing amount of Mo species. The decrease in S_{BET} can originate from a coalescence process, since sintering can be favoured in the presence of dopants.

The ZPCs of the studied catalysts was decreasing with an increasing Mo content, probably due to the continuous TiO_2 surface enrichment with acidic species (different Mo_xO_y).

Table 3
Characterization of TiO₂ and x wt% Mo/TiO₂ catalysts.

Catalyst	Real metal content (%) ^a	S _{BET} (m ² /g) ^b	V _p (cm ³ /g) ^b	D _p (nm) ^b	ZPC ^c	Band gap (eV) ^d
TiO ₂	–	57	0.429	37.5	6.6	3.09
0.5 wt% Mo/TiO ₂	0.52	56.5	0.413	36.0	6.3	2.90
1 wt% Mo/TiO ₂	0.99	56.1	0.430	37.6	6.0	2.90
2 wt% Mo/TiO ₂	2.02	55.1	0.427	38.1	4.3	2.85
3 wt% Mo/TiO ₂	3.01	53.0	0.426	29.1	3.1	2.91
5 wt% Mo/TiO ₂	5.02	51.0	0.424	28.6	2.5	2.95

S_{BET}: Specific surface area determined by BET method; V_p: pore volume taken at p/p₀ = 0.99; D_p: average pore diameter determined by the BJH method.

^a Determined by AAS.

^b Determined by N₂-BET.

^c Determined by MT.

^d Determined by UV–VIS DRS.

Moreover, under increasing Mo content, the diffuse reflectance spectra reveal a red shift in the band gap of TiO₂ into lower eV (Table 3), with a minimum value of 2.85 obtained for 2 wt% Mo/TiO₂. This is due to the introduction of energy levels of Mo species into the band gap of TiO₂. However, the further increase in Mo content (3 and 5 wt%) led to an increase in the band gap. It can be related to the MoO₃ formation on TiO₂ surface considering that the molybdate anions bind very strongly to the titania surface and that they can be hindered during the calcination of the catalysts. It should be noted that the band gap of MoO₃ equals 3.0 [9,23].

SEM–EDS micrographs of TiO₂ and Mo/TiO₂ catalysts are presented in Appendix 1. Any significant differences in the morphology of TiO₂ and Mo/TiO₂ catalysts can be seen. The EDS measurements confirmed Mo presence. All samples contained the aggregates with irregular shapes and sizes in the range of 2–30 μm. The following order of average size of catalysts agglomerates, depending on the Mo loading, was observed: 2 wt% Mo/TiO₂ (2 μm) < 1 wt% Mo/TiO₂ (5 μm) < 0.5 wt% Mo/TiO₂ (8 μm) < 3 wt% Mo/TiO₂ (10 μm) < 5 wt% Mo/TiO₂ (12 μm) < TiO₂ (30 μm). For the catalysts with Mo content in the range of 0.5–2 wt%, SEM–EDS images revealed very uniform distribution of Mo on the TiO₂ surface. For the samples with higher Mo content, rough metal distribution with characteristic agglomerations was observed.

The XRD patterns of different Mo/TiO₂ catalysts (not shown here) did not reveal neither clear Mo nor molybdenum oxides reflections, even for the catalyst containing the highest Mo loading. It could be related to

the amorphous nature of Mo-containing species and/or their random spread on TiO₂ surface.

A negligible effect of increasing Mo content on TiO₂ lattice parameters was also observed (Table 4), confirming the presence of metal on the support surface instead of its incorporation into the TiO₂ lattice. The slight increase in the crystallite size of Mo/TiO₂ catalysts with an increase in Mo content was observed, due to the catalysts sintering and/or Mo–O–Ti bonds formation. Moreover, the anatase fraction as well as anatase to rutile ratio was higher for the samples containing the highest Mo loading (3 and 5 wt%). It means that the increasing Mo content inhibit the anatase to rutile phase transformation.

Fig. 5 shows the Raman spectra of x wt% Mo/TiO₂ catalysts. The observed species together with their respective peak frequencies are summarized in Table 5. The corresponding analysis was performed for the selected part of the spectra (wave number range of 800–1000 cm⁻¹) in which peaks characteristic of different Mo_xO_y are expected. One can see that depending on Mo loading, different Mo_xO_y species on titania surface were registered. The catalysts with low Mo content are characterized by the presence of structures based on [Mo₇O₂₄]⁶⁻ ion (0.5 wt% Mo/TiO₂), or on the mixture of phases based on [Mo₇O₂₄]⁶⁻ and [Mo₅O₁₇]⁴⁻ ions and Mo₅O₁₄ (1 wt% Mo/TiO₂). Under increasing amount of Mo, the intensity of the phases based on [Mo₅O₁₇]⁴⁻ ion increases. Moreover, new phases based on [Mo₇O₂₄]⁶⁻ ion and Mo₄O₁₁ are detected (2 wt% Mo/TiO₂). Further increase in Mo loading (3 wt% Mo/TiO₂) results in the formation of additional phases based on [Mo₈O₂₆]⁴⁻, or

Table 4
The average crystallite size, lattice parameters and anatase to rutile ratio of TiO₂ and x wt% Mo/TiO₂ catalysts.

Catalyst	d _{hkl} (Å)	a = b (Å)	c (Å)	Cell volume (Å ³)	Crystallite size (nm)	Anatase fraction (%)	Anatase/rutile ratio
TiO ₂ (as received)	3.5	3.8	9.8	140.4	20.7	84.95	5.6
0.5 wt% Mo/TiO ₂	3.5	3.8	9.4	134.6	20.0	84.8	5.6
1 wt% Mo/TiO ₂	3.5	3.8	9.4	133.8	20.6	83.7	5.1
2 wt% Mo/TiO ₂	3.5	3.8	9.8	141.9	21.0	84.5	5.5
3 wt% Mo/TiO ₂	3.5	3.8	9.5	137.1	21.4	87.9	7.3
5 wt% Mo/TiO ₂	3.5	3.8	9.6	138.3	21.7	89.4	8.4

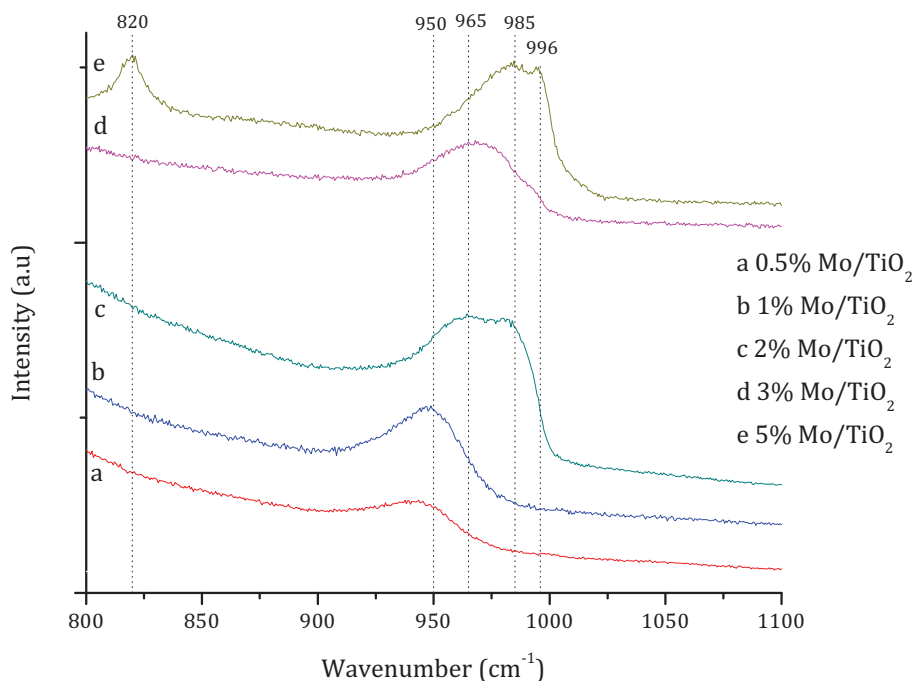


Fig. 5. (Color online.) Representative Raman spectra for different x wt% Mo/TiO₂ catalysts.

structures based on double cell [Mo₅O₁₇]⁴⁻, therefore [Mo₁₀O₃₄]⁸⁻. Finally, for the sample impregnated with the highest amount of Mo (5 wt% Mo/TiO₂), the new peaks at 820 cm⁻¹ (ν_s Mo=O stretching) and at 996 cm⁻¹ (ν_{as} Mo=O stretching) were observed. They are characteristic of the presence of MoO₃.

Fig. 6a resumes the results of phenol photo-degradation under UV radiation in the presence of TiO₂ or x wt% Mo/TiO₂. Under increasing Mo loading, the percentage of phenol degradation increases with the maximum achieved over 2 wt% Mo/TiO₂ (96.2%), which was found to be higher than that corresponding to bare TiO₂ (89.6%).

However, further increase in Mo content leads to the decrease in the photoactivity of the catalysts. Similar order of activity was observed under visible light (Fig. 6b): 2 wt% Mo/TiO₂ (14.3%) > TiO₂ (11.4%) > 1 wt%

Mo/TiO₂ (11%) > 3 wt% Mo/TiO₂ (4.6%) > 5 wt% Mo/TiO₂ (3.9%) > 0.5 wt% Mo/TiO₂ (2.9%).

The acid–base properties of the studied catalysts cannot be directly correlated with their activity results. However, they can affect the extent of phenol adsorption on TiO₂ surface and consequently its photoactivity. At the catalyst's ZPC, its interaction with water contaminant is minimal due to the absence of any electrostatic force. Thus, the surface of catalysts with ZPC higher than 5 (pH of reaction), i.e. 0.5–1 wt% Mo/TiO₂, becomes positively charged (e.g., TiOH₂⁺); meanwhile the molecule of phenol is a non-dissociated one (neutral, pK_a = 9.95). On the other hand, the surface of catalysts with ZPC significantly lower than 5 (pH of reaction), i.e. 3–5 wt% of Mo/TiO₂, will be negatively charged (e.g., TiO⁻) and repulse the phenolate ions (C₆H₅O⁻) in water. Thus, one can see that the phenol degradation is higher for the catalysts with ZPC close to the pH of the treated solution.

The differences in the photoactivity of Mo/TiO₂ catalysts can be also attributed to their morphology. One can see that the decrease in S_{BET} and mean pore size diameter as well as increase in catalyst agglomerate size, under increasing Mo content, was detrimental for the photoactivity.

The diffuse reflectance spectra revealed a red shift in the band gap transition under an increasing amount of Mo impregnated on TiO₂ surface (Table 3). According to the literature [15], it can be related to the introduction of Mo energy levels into the band gap of TiO₂. Thus, the presence

Table 5
Raman peak frequencies for different Mo_xO_y species.

Species	Wavenumber (cm ⁻¹)		Reference
	800–900	900–1000	
MoO ₃	820	996	[24]
Mo ₄ O ₁₁	835, 843	907, 985	[20]
[Mo ₇ O ₂₄] ⁶⁻	893	908, 919, 938	[20]
[Mo ₅ O ₁₇] ⁴⁻	893	922, 930, 935, 948	[20]
[Mo ₈ O ₂₆] ⁴⁻	889	911, 932, 951, 965	[20]
[Mo ₁₀ O ₃₄] ⁸⁻		909, 969	[20]
Mo ₅ O ₁₄	898	930, 950	[20]

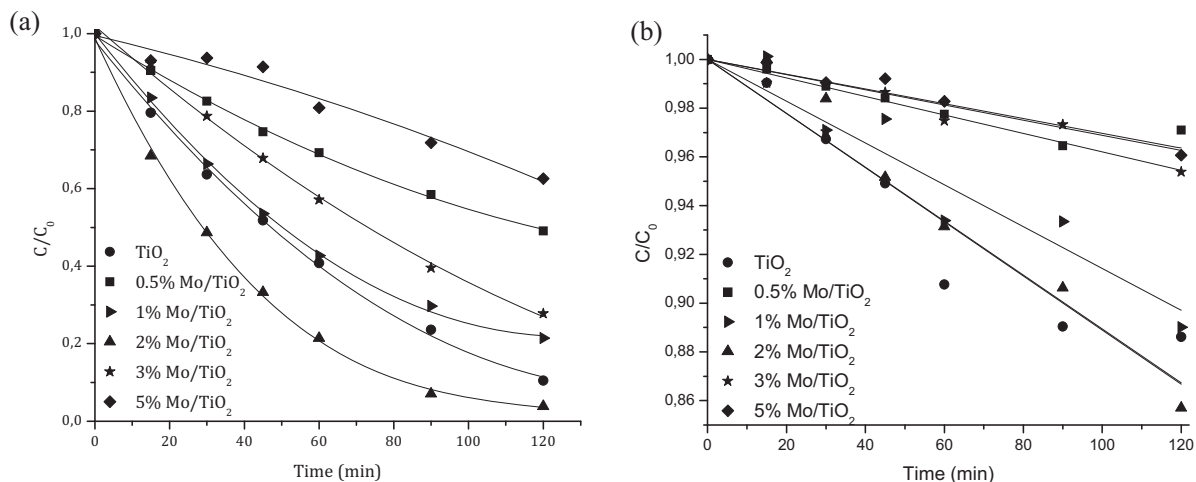


Fig. 6. Photocatalytic degradation of phenol over TiO_2 and x wt% Mo/TiO_2 catalysts under: (a) UV radiation and (b) visible light ($C_{\text{phenol}} = 20$ ppm, $\text{pH} = 5$, $C_{\text{cat}} = 0.5$ g/L).

of new energy levels, below the conduction band edge and above the valance band edge, can affect catalyst photoactivity since Mo ions can act as electron-hole pair recombination centers, according to the following reactions:



where e^- and h^+ correspond to electron and positively charged hole, respectively. Therefore, as the concentration of Mo increases, the space-charge region becomes narrower and the electron-hole pairs within the region can be efficiently separated by the large electric field before recombination. On the other hand, if the concentration of Mo is too high, the space-charge region becomes very narrow and the light penetration depth into catalyst greatly exceeds the space-charge layer. Therefore, the recombination of photogenerated electron-hole pairs in the catalyst increases, due to the lack of driving force to separate them [15]. The optimum concentration of Mo ions makes the thickness of space-charge layer equal to the light penetration depth and in this case is 2 wt%.

Finally, a relation between phenol degradation percentage and Mo_xO_y species present on the TiO_2 surface can be found. Under increasing Mo content, the appearance of different Mo_xO_y species was registered. However, the coverage of TiO_2 surface with bulk MoO_3 was observed only for 5 wt% Mo/TiO_2 , a catalyst characterized by the lowest phenol degradation percentage.

Therefore, high activity of 2 wt% Mo/TiO_2 can be attributed to the synergetic effect between S_{BET} , mean pore size diameter, catalyst agglomerate size, band gap, ZPC, and the type of Mo_xO_y species on TiO_2 surface.

4. Conclusions

Photocatalytic degradation of phenol under both UV radiation and visible light, using TiO_2 (Degussa P-25) and TiO_2 loaded with some transition metal ions (Co, Cu, Fe and Mo) was examined. The most significant results can be summarized as follows:

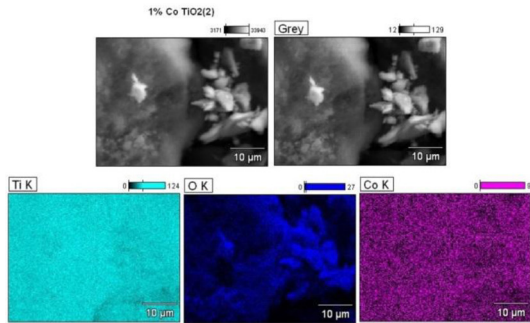
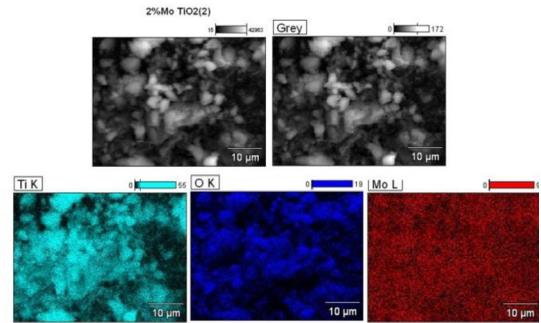
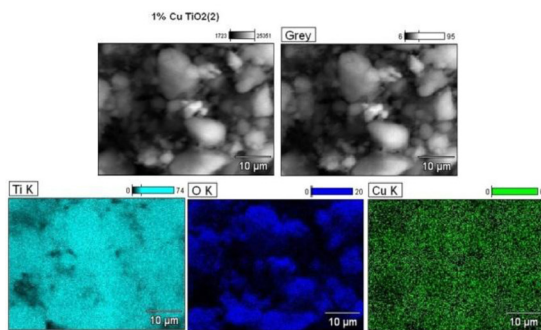
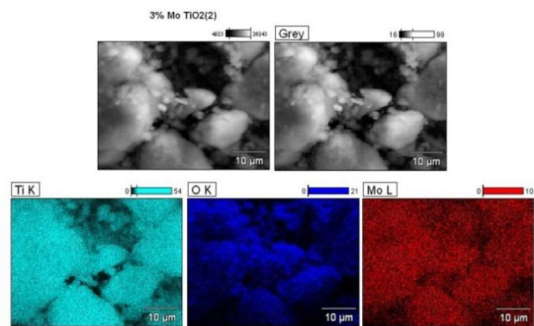
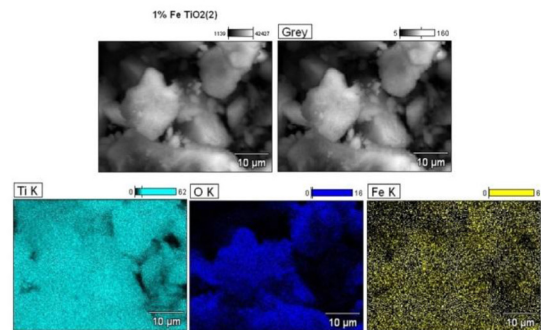
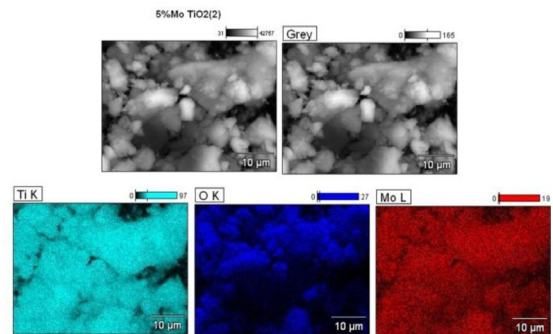
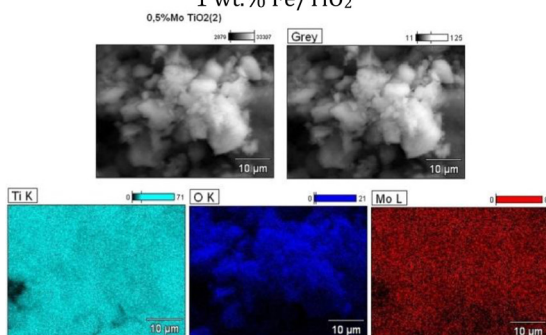
- from the series of metal loaded catalysts, Mo/TiO_2 was the most efficient one. Its photocatalytic performance was attributed to the synergetic effect between S_{BET} , mean pore size diameter, catalyst agglomerate size, band gap and ZPC. In the presence of Mo, neither TiO_2 anatase/rutile fraction nor its pore size diameter has been affected. However, Mo made its surface more acidic. The percentage of phenol degradation reached under visible light was significantly lower than that under UV radiation due to the lower degree of light absorption by the catalyst surface;
- from the series of studied x wt% Mo/TiO_2 catalysts, 2 wt% Mo/TiO_2 was the most effective one. The synergetic effect between S_{BET} , mean pore size diameter, catalyst agglomerates size, band gap, ZPC and the type of Mo_xO_y species on TiO_2 surface, depending on Mo loading, created its photocatalytic performance.

Acknowledgments

The financial support of COLCIENCIAS and Universidad Nacional de Colombia, Sede Manizales (Programa Jóvenes Investigadores e Innovadores Convocatoria 525 de 2011 – Convenio Especial de Cooperación No. 0043 de 2012) is gratefully acknowledged. This work was partially supported by DIMA–Apoyo a Tesis de Posgrado 2012 (project 15932) and the program of Semilleros de Investigación en Pregrado (Res. CFCEN-100 del 15.09.2010).

Appendix 1.

The back-scattered electron (BSE) photomicrographs and EDS maps of studied catalysts. (Magnification: $\times 2500$).

1 wt.% Co/TiO₂2 wt.% Mo/TiO₂1 wt.% Cu/TiO₂3 wt.% Mo/TiO₂1 wt.% Fe/TiO₂5 wt.% Mo/TiO₂0.5 wt.% Mo/TiO₂

References

- [1] E. Grabowska, J. Reszczyńska, A. Zaleska, *Water Res.* 46 (2012) 5453.
- [2] S. Ahmed, M.G.G. Rasul, W.N. Martens, R. Brown, M.A. Hashib, *Desalination* 261 (2010) 3.
- [3] C. Adán, A. Bahamonde, M. Fernández-García, A. Martínez-Arias, *Appl. Catal. B, Environ.* 72 (2007) 11.
- [4] A. DiPaola, G. Marci, E. García-López, C. Martín, L. Palmisano, V. Rives, A.M. Venezia, *Appl. Catal. B, Environ.* 48 (2004) 223.
- [5] L. Gomathi Devi, K. Eraiah Rajashekhar, *J. Mol. Catal. A, Chem.* 334 (2011) 65.
- [6] P. Górska, A. Zaleska, J. Hupka, *Sep. Purif. Technol.* 68 (2009) 90.
- [7] A.V. Emeline, X. Zhang, T. Murakami, A. Fujishima, *J. Hazard. Mater.* 211–212 (2012) 154.
- [8] S.-H.H. Lin, C.-H.H. Chiou, C.-K.K. Chang, R.-S.S. Juang, *J. Environ. Manage.* 92 (2011) 3098.
- [9] S.M. López-Zamora, *Synthesis and Characterization of Modified TiO₂ for the Photo-Treatment of Wastewater with Visible Light*, Universidad Nacional de Colombia, 2013.
- [10] A. DiPaola, G. Marci, S. Ikeda, B. Ohtani, L. Palmisano, *Int. J. Photoenergy* 3 (2001) 171.
- [11] A. DiPaola, G. Marci, L. Palmisano, S. Ikeda, B. Ohtani, M. Schiavello, K. Uosaki, *J. Phys. Chem. B* 106 (2002) 637.
- [12] L. Baia, L. Diamandescu, L. Barbu-Tudoran, A. Peter, G. Melinte, V. Danciu, M. Baia, *J. Alloys Compd.* 509 (2011) 2672.
- [13] Y. Yalçi, M. Kiliç, Z. Çınar, M. Kılıç, Z. Çınar, *Appl. Catal. B, Environ.* 99 (2010) 469.
- [14] S. Rehman, R. Ullah, A.M. Butt, N.D. Gohar, *J. Hazard. Mater.* 170 (2009) 560.
- [15] O. Carp, C.L. Huisman, A. Reller, *Prog. Solid State Chem.* 32 (2004) 33.
- [16] D.A.H. Hanaor, C. Sorrell, *J. Mater. Sci.* 46 (2011) 855.
- [17] F. Bregani, C. Casale, L.E. Depero, I. Natali-Sora, D. Robba, L. Sangaletti, G.P. Toledo, *Sens. Actuators B* 31 (1996) 25.
- [18] B. Jongsomjit, C. Sakdamnusun, J.G. Goodwin Jr., P. Praserttham, *Catal. Lett.* 94 (2004) 209.
- [19] Y. Saih, K.S. Å, K. Segawa, *Catal. Surv.* 7 (2003) 235.
- [20] M. Dieterle, *In Situ Resonance Raman Studies of Molybdenum Oxide Based Selective Oxidation Catalysts*, Technical University of Berlin, 2001.
- [21] M.S.P. Francisco, V.R. Mastelaro, *Chem. Mater.* 14 (2002) 2514.
- [22] D.-L.A. De Faria, S. Vena, *J. Raman Spectrosc.* 28 (1997) 873.
- [23] S. Chen, L. Wang, *Chem. Mater.* 24 (2012) 3659.
- [24] K.Y.S. Ng, E. Gulari, *J. Catal.* 92 (1985) 340.